Picosecond electron deflectometry of optical-field ionized plasmas

MARTIN CENTURION[1]*†, PETER RECKENTHAELER[1,2]†, SERGEI A. TRUSHIN[1], FERENC KRAUSZ[1,2] AND ERNST E. FILL[1]

[1]Max-Planck-Institut für Quantenoptik, Hans-Kopfermann-Strasse 1, D-85748 Garching, Germany
[2]Ludwig-Maximilians-Universität München, Am Coulombwall 1, D-85748 Garching, Germany
†These authors contributed equally to this work.
*e-mail: martin.centurion@mpq.mpg.de

Published online: 20 April 2008; doi:10.1038/nphoton.2008.77

Optical-field ionized plasmas are of great interest owing to their unique properties and the fact that they suit many applications, such as the study of nuclear fusion[1], generation of energetic electrons[2–5] and ions[6,7], X-ray emission[8,9], X-ray lasers[10–12] and extreme-UV attosecond pulse generation[13]. A detailed knowledge of the plasma dynamics can be critical for optimizing a given application. Here we demonstrate a method for real-time imaging of the electric-field distribution in optical-field ionized plasmas with ultrahigh temporal resolution, yielding information that is not accessible by other methods. The technique, based on electron deflectometry, yields images that reveal a positively charged core and a cloud of electrons expanding far beyond the Debye length.

The parameters of an optical-field ionized (OFI) plasma can be varied over a wide range. The maximum ionization stage can be set by the intensity of the laser pulse generating the plasma[14], the electron temperature can be controlled by applying linear or circular polarization[15], and, by appropriately choosing the backing pressure of the nozzle, cluster plasmas[16] can be generated. Various methods have been applied to investigate the parameters of OFI plasmas. The electron temperature has been measured by Thomson scattering[17]. The ionization stage has been determined by ion spectrometry[18] and by recording the emission of X-rays from the plasma[11]. The time-resolved plasma density profile has been measured by optical interferometry and holography[19,20]. Moiré deflectometry has been used to determine the density profile in the plasma channel and its lateral expansion[21]. Spectrometry of ions emitted from the plasma has yielded information on ion velocity and temperature[22]. Radiography using energetic (MeV) protons has been used to diagnose density perturbations and transient fields in high-density plasmas with a temporal resolution of 100 ps (refs 23–25).

Here, we demonstrate a new diagnostics technique for OFI plasmas with a temporal resolution of 2.7 ps and very high sensitivity. The technique is deflectometry using monoenergetic 20-keV electron pulses, which are directed onto an OFI nitrogen plasma generated by a 50-fs Ti:sapphire laser pulse. The electrons are deflected by the fields resulting from charge separation, and the resulting distortion of the electron beam yields time-resolved images of the plasma. Pump–probe experiments on the plasma evolution capture changes within a few picoseconds, with a spatial resolution of 30 μm. This direct time-resolved imaging of plasma fields reveals features not accessible to other methods. Such knowledge can help to improve the setting of parameters for optimizing particular applications. As an example, X-ray lasers and soft X-ray sources may greatly benefit from a better understanding of the dynamics of laser-generated plasmas. The new technique has the potential to lead to better control of plasma electron and ion accelerators and improve their features. The high sensitivity of electron deflectometry is based on the fact that even small charge imbalances within the plasma are observable as distortions in the spatial profile of the electron beam. The narrow energy spread and low emittance ($\varepsilon = 1.5$ mrad mm) of the electron beam allows plasma fields below $1 \times 10^6\,\mathrm{V\,m^{-1}}$ to be detected.

An application of the method is illustrated in Fig. 1, which shows the evolution of a nitrogen OFI plasma. Initially, a small depleted region appears in the electron beam in the area of the laser focus. This hole expands for approximately 80 ps, after which a spot develops in the centre (Fig. 1e,f). The spot becomes brighter than the initial electron beam for a time delay $T > 100$ ps, and its intensity increases up to 200 ps. Beyond 200 ps (not shown in the figure) the brightness of the spot slowly decreases.

Simultaneously with the depleted region, two bright lobes appear on each side of the plasma region, along the line of laser propagation (vertical in Figs 1 and 2). These lobes then move away from the focal region in opposite directions. The sidelobes reach the boundary of the electron beam after approximately 100 ps (Fig. 1e) and then remain static. The pattern remained qualitatively unchanged until the maximum delay time in the experiment ($T = 300$ ps), with only a slight decrease in the brightness of the main features.

Figure 2 focuses on the initial stages of the plasma expansion. The duration of the electron pulses was decreased by reducing the number of electrons per pulse. Figure 2a–d shows the plasma evolution with a step size of $\sim$2.7 ps. The formation of an expanding feature is clearly visible after the first step. After only 5.3 ps (Fig. 2c) there is already a well-defined boundary and deflected electrons appear in the shadow of the nozzle. For $T > 5.3$ ps (Fig. 2d–i) the hole expands and the number of electrons deflected out of the focal region increases. The sidelobes at the boundary of the plasma also appear at 5.3 ps (Fig. 2c), then increase in brightness and move away from the centre. At $T = 24$ ps (Fig. 2g) the fraction of electrons ejected reaches its

© 2008 Nature Publishing Group

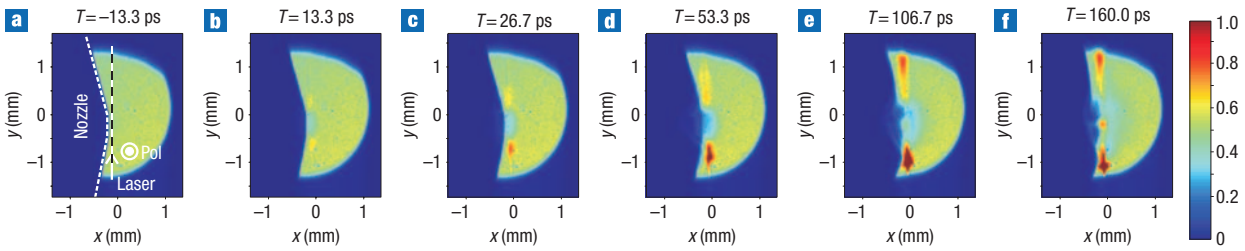

Figure 1 Pump–probe images of plasma evolution. a–f, Changes in the electron beam due to the charge distribution in the plasma as a function of the time delay T between the electron and laser pulses. The dark area in the left part of the images is the shadow of the gas nozzle. The geometry is included as an overlay in **a.** The laser is incident from below with a polarization (pol) perpendicular to the image plane, the width of the black and white dashed line in **a** corresponding to the maximum width of the laser beam while traversing the electron beam, and the position of the line corresponding to the path of the laser. The colour mapping represents the number of electron counts normalized to the maximum.

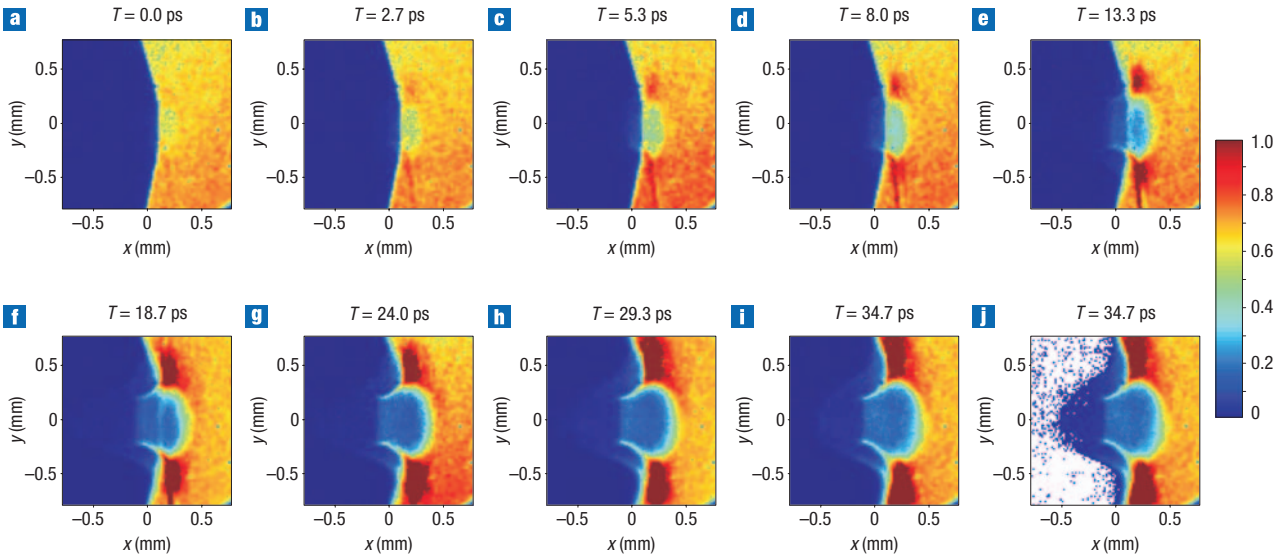

Figure 2 High-resolution pump–probe images. a–i, Images of plasma evolution with increasing time delay. **j**, Image for the same time delay (34.7 ps) as in **i**, with the colour corresponding to the lowest number of counts (dark blue) removed to highlight the pattern of deflected electrons. The geometry is the same as shown in Fig. 1a. The colour mapping represents the number of electron counts normalized to the maximum.

maximum of 80% and additional deflected electrons are observed in the shadow of the nozzle, with a maximum deflection angle of 8 mrad. Figure 2j shows the pattern at 34.7 ps with the background colour (dark blue) removed to highlight the deflected electrons. Note the sharp boundary on the right side of the plasma, which at 24 ps (Fig. 2g) has a width of about 0.2 mm. For $T > 70$ ps (not shown in Fig. 2) a bright spot appears in the centre of the focal region and the sharp boundary of the expanding region slowly diffuses. The velocity of the expanding feature (moving to the right) calculated from the data is $v = 4.9 \times 10^6\,\mathrm{m\,s^{-1}}$. The velocity remained constant from $T = 10$ ps to $T = 70$ ps, after which time the boundary is no longer well defined.

We attribute the depleted region in the electron beam to strong deflection of the beam electrons by net positive charges in the central region and an expanding cloud of hot electrons. Within the cloud of electrons the field rapidly decreases and the radius increases. In the region where the electrons fully screen the positive charge the field vanishes. We note that the electron-cloud radius is two orders of magnitude larger than the Debye length of the plasma, far beyond what is expected from a simple model of charge separation. The generation of such a charge distribution is only possible if a small fraction of the electrons acquires a significantly higher energy than the bulk of the plasma electrons. Several mechanisms exist through which a small fraction of the electrons may acquire an energy close to or even exceeding the ponderomotive potential of the laser at the focus (250 eV in our experiment). The most important of these are heating of electrons through re-collisions[26] and sequential multi-electron emission[27]. The moving sidelobes are generated by deflection due to magnetic fields near the boundaries of the gas jet, and by ionization of background gas.

For the quantitative analysis of the patterns, the equation of motion for the expanding electrons in their self-generated electric field, E, was numerically solved in a lagrangian coordinate system[28]. A quasi-two-dimensional cylindrical model was used, where the electrons expand only radially, and the number and initial temperature of the electrons depend on the axial

© 2008 Nature Publishing Group

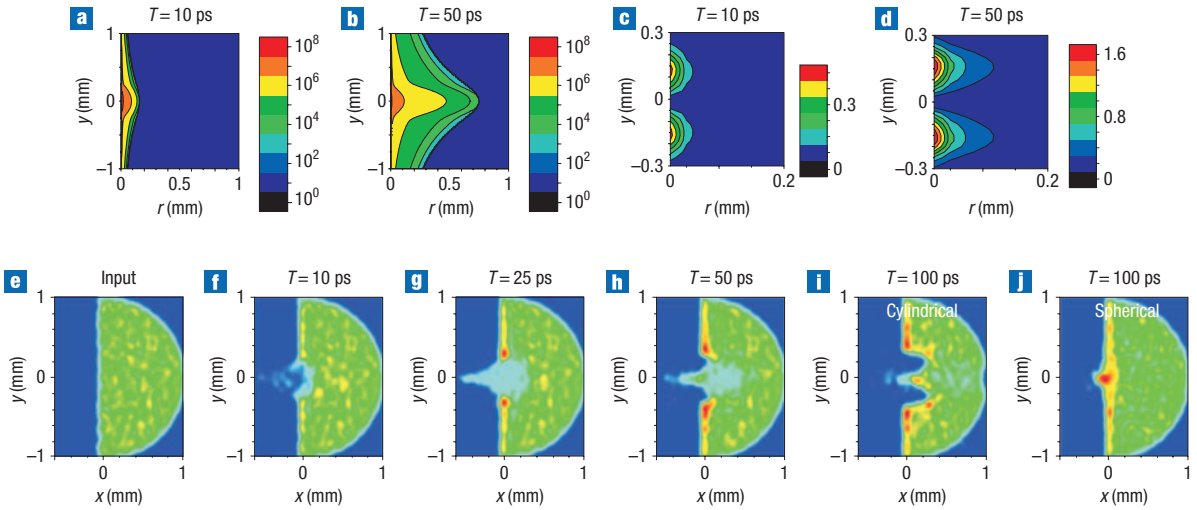

Figure 3 Calculated plasma fields and simulated beam. a,b Contours of the radial E field in a cylindrical geometry for delays of 10 ps (**a**) and 50 ps (**b**). The colour scale denotes $\log_{10}$ of the field in units of $\mathrm{V\,m^{-1}}$. **c,d**, Azimuthal B field, in units of tesla for delays of 10 ps (**c**) and 50 ps (**d**). **e**, Input electron beam (diameter 2 mm) used for the simulations. **f–i**, Simulated beam pattern at the detector for delays of 10 ps (**f**), 25 ps (**g**), 50 ps (**h**) and 100 ps (**i**) with a cylindrical symmetry. **j**, Beam pattern at 100 ps delay applying the simulation with a spherical symmetry.

position y (distance from the focus along the propagation direction of the laser). The corresponding magnetic field, B, is calculated by the time integral of the curl of the E field. The pattern on the detector for a given time delay was then simulated by propagating a 20-keV electron beam through the previously calculated fields using the GPT (General Particle Tracer) code (http://www.pulsar.nl.net), a well-established simulation tool for particle propagation. The choice of cylindrical geometry is motivated by the experimental parameters: the laser beam (focus diameter, 20 μm; Rayleigh length, 600 μm) generates a thin plasma wire through the gas jet (radius, 150 μm). A background gas density of 5% is also included in the calculations. The initial plasma density and electron temperature are proportional to the gas density and laser intensity, respectively, both of which depend on the position along the y axis (see Fig. 1a). The best agreement between experiment and simulation was achieved for 5×10^7 charges (5×10^{-4} of the total number of electrons in the plasma), and hot electrons with an exponential energy distribution and a temperature of 250 eV.

Figure 3a,b shows contour plots of the calculated radial E field for $T = 10$ ps and $T = 50$ ps, in $\log_{10}$ scale. The expanding E field leads to an expanding depleted region in the electron-beam pattern as more electrons are deflected. The field reaches a value of $1 \times 10^8\,\mathrm{V\,m^{-1}}$ at the centre of the gas jet ($y = 0$) where the density is highest, and decreases with radial distance from the positive charges. The corresponding B field (Fig. 3c,d) is azimuthal owing to the cylindrical symmetry, and appears initially in the regions of high density gradient. There is a partial cancelling of the deflection due to the azimuthal B field, with a net deflection along y, away from the regions of high B field.

Figure 3e–j shows the simulated patterns. The left side of the electron beam is blocked to simulate the effect of the nozzle, which allows the deflected electrons to be seen. Electrons are initially deflected out of the central region by the E field, with a maximum deflection angle of 9 mrad, in good agreement with the measured value. A weak line is visible along the laser trajectory, which corresponds to expansion of the electrons from the plasma generated in the background gas. For $T > 10$ ps (Fig. 3g–i), the B field also contributes to the depletion by deflecting electrons along y, which generates the sidelobes. As the fields evolve in time, the sidelobes move away from the centre owing to the B field, and the depleted region grows owing to the combined effect of the E and B fields, again in good agreement with experiment. In the experiment (Fig. 1) there is an asymmetry in the brightness of the sidelobes, with the one on the side of the outgoing laser being weaker, possibly due to absorption of the laser across the gas jet. In the simulations the absorption of the laser is not included; thus the asymmetry does not appear. For $T \geq 100$ ps, the expansion is no longer cylindrical, as the electrons have expanded well beyond the initial length of the plasma wire (the diameter of the gas jet), and the experimental pattern (Fig. 1) shows a combination of cylindrical and spherical features. A full three-dimensional model would be necessary to fully reproduce the experiment in this case; however, we show that the main features are captured by two separate simulations, with cylindrical and spherical symmetry (Fig. 3i,j). The sidelobes and depleted region are reproduced in the cylindrical case, and the round focused spot in the centre appears in the spherical case. The pattern in the case of spherical symmetry remains relatively unchanged up to 200 ps. The focused spot can best be explained by a positively charged core and a spherical cloud of expanding electrons. In summary, our simulations capture the main features of the experiment, with good agreement for the early stages and qualitative agreement for the later stages, and allow the fields, total charge and electron temperature to be calculated.

In conclusion, we have demonstrated a new method of imaging OFI plasmas with picosecond temporal resolution. New features of OFI plasma were observed using this method, such as a cloud of electrons separating from the plasma core far beyond the Debye length. Additionally, we have observed the effect of both electric and magnetic fields on the probe electron beam. The relevant physical parameters, such as the fields, number of charges and electron temperature, were calculated numerically. The sensitivity of subrelativistic electrons to relatively small fields makes this method applicable to the investigation of the dynamics of low-density plasmas.

© 2008 Nature Publishing Group

METHODS

ELECTRON-PULSE GENERATION

The electron pulses were generated by laser pulses incident on a photocathode. The laser pulses were linearly polarized at a central wavelength of 800 nm, with a temporal full-width at half-maximum of 50 fs, a repetition rate of 1 kHz and an energy of 1.8 mJ. A small fraction of the laser light was split from the main beam and focused onto the surface of a copper cathode inside the acceleration chamber. Electrons were emitted from the surface by means of a three-photon photoelectric effect and then accelerated to 20 keV. The energy bandwidth due to the initial energy of the electrons and space-charge effects is expected to be well below 10 eV.

RESOLUTION LIMITS

The main parameter limiting the sensitivity as well as the spatial resolution of our method is the emittance ε of the electron beam. The minimum field that can be measured in a particular experiment can be estimated by comparing the angular spread $\Delta\varphi_\varepsilon = \varepsilon/r_b$ of electron trajectories due to the emittance to the deflection angle $\Delta\varphi_E = El_p/2U_b$ of an electron in a plasma field E. In these equations r_b denotes the radius of the electron beam, l_p the length of the plasma and U_b the energy of the beam electrons in eV. The emittance of our electron beam was determined by evaluating the blurring of the shadow of a sharp aperture, resulting in $\varepsilon = 1.5$ mrad mm. Taking $l_p = 50\ \mu$m, 20-keV electrons allow fields down to $6.7 \times 10^5\ \mathrm{V\,m^{-1}}$ to be measured. Such a field occurs at a distance of 100 μm from a charged core with a charge of about a pC.

The spatial resolution is also limited ultimately by the emittance of the electron beam. Using the blurring of a sharp spatial structure by the beam emittance, the minimum resolvable distance between two spots is $\Delta x = \varepsilon L/r_b$, where L is the distance between the plasma and the detector. The resolution can be improved by using an expanding beam. If M is the magnification achieved at the detector the corresponding relation is $\Delta x = \varepsilon L/Mr_b$. Note the tradeoff between spatial resolution and detectable field: the spatial resolution increases with decreasing L, but the field sensitivity suffers because $\Delta\varphi_E L$ decreases and may even become smaller than the minimum resolvable structure on the detector.

The temporal resolution of our experiment may be improved by using a shorter electron pulse, which can be accomplished by using fewer electrons per pulse and reducing the propagation distance to the target. Additionally, the resolution is also limited by the velocity mismatch between the laser pulse and the subrelativistic electron pulse. For 20-keV electrons and a 100-μm plasma the time difference amounts to 900 fs. By increasing the electron energy this mismatch can be eliminated, but at the cost of field sensitivity.

PLASMA GENERATION

The main part of the laser beam is expanded and then focused with a lens with a focal distance, $f = 300$ mm into a nitrogen gas jet to a spot 20 μm in diameter, resulting in a peak intensity of $4 \times 10^{15}\ \mathrm{W\,cm^{-2}}$. At the point of plasma generation, the gas jet has a density of $2.4 \times 10^{17}\ \mathrm{cm^{-3}}$ as measured by evaluating the reduction in electron-beam intensity after traversing the jet. The temporal delay between the pump laser and electron pulses is adjusted by means of a motorized stage.

DATA ACQUISITION AND PROCESSING

The number of electrons per pulse is determined by means of a Faraday cup coupled to a picoammeter. It can be controlled by the intensity of the laser beam on the cathode. We used 65,000 electrons per pulse for the acquisiton of Fig. 1 and 2,300 electrons per pulse for Fig. 2. The GPT simulations predict 15-ps and 2.6-ps electron pulses respectively for these parameters. Images are recorded by means of a phosphor-coated fibre plate coupled to a CCD chip. Residual laser light is rejected by a 100-nm aluminium layer on the phosphor coating. The divergence of the electron beam results in a magnification factor of 1.6. The spatial resolution of the imaging system is estimated as 50 μm.

Images were acquired on the CCD with integration times of 1 s for the images in Fig. 1 and 3 s in Fig. 2, corresponding to 1,000 and 3,000 electron pulses, respectively. An image of the electron beam without the laser beam was used to correct a gradient in the intensity of the electron beam. A background image without the electron beam was used to subtract the residual scattered laser light.

NUMERICAL SIMULATION

For calculating the pattern on the detector, the GPT code, a well-established simulation tool for particle propagation, was applied. A beam of 5,000 electrons with $U_b = 20$ keV was simulated propagating through the fields generated by the simulations of the expanding electron cloud. To take the nozzle properly into account a scatterplate was inserted, obscuring the beam at 100 μm to the left of the centre.

Received 18 December 2007; accepted 18 March 2008; published 20 April 2008.

References

1. Ditmire, T. *et al.* Nuclear fusion from explosions of femtosecond laser-heated deuterium clusters. *Nature* **398,** 489–492 (1999).
2. Baton, S. D. *et al.* Evidence of ultrashort electron bunches in laser–plasma interactions at relativistic intensities. *Phys. Rev. Lett.* **91,** 105001 (2003).
3. Davies, J. R., Bell, A. R. & Tatarakis, M. Magnetic focusing and trapping of high-intensity laser-generated fast electrons at the rear of solid targets. *Phys. Rev. E* **59,** 6032–6036 (1999).
4. Geddes, C. G. R. *et al.* High-quality electron beams from a laser wakefield accelerator using plasma-channel guiding. *Nature* **431,** 538–541 (2004).
5. Wilks, S. C., Kruer, W. L., Tabak, M. & Langdon, A. B. Absorption of ultra-intense laser pulses. *Phys. Rev. Lett.* **69,** 1383–1386 (1992).
6. Ditmire, T. *et al.* High-energy ions produced in explosions of superheated atomic clusters. *Nature* **386,** 54–56 (1997).
7. Wei, M. S. *et al.* Ion acceleration by collisionless shocks in high-intensity-laser–underdense-plasma interaction. *Phys. Rev. Lett.* **93,** 155003 (2004).
8. Fill, E. *et al.* XUV spectra of optical-field-ionized plasmas. *Phys. Rev. E* **51,** 6016–6026 (1995).
9. McPherson, A., Luk, T. S., Thompson, B. D., Boyer, K. & Rhodes, C. K. Multiphoton-induced X-ray emission and amplification from clusters. *Appl. Phys. B* **57,** 337–347 (1993).
10. Amendt, P., Eder, D. C. & Wilks, S. C. X-ray lasing by optical-field-induce ionization. *Phys. Rev. Lett.* **66,** 2589–2592 (1991).
11. Lemoff, B. E., Yin, G. Y., Gordon III, C. L., Barty, C. P. J. & Harris, S. E. Demonstration of a 10-Hz femtosecond-pulse-driven XUV laser at 41.8 nm in Xe IX. *Phys. Rev. Lett.* **74,** 1574–1578 (1995).
12. Nagata, Y. *et al.* Soft-X-ray amplification of the Lyman-alpha transition by optical-field-induced ionization. *Phys. Rev. Lett.* **71,** 3774–3777 (1993).
13. Bandrauk, A. D., Chelkowski, S. & Nguyen, H. S. Nonlinear photon processes in molecules at high intensities—route to XUV-attosecond pulse generation. *J. Mol. Structure* **735,** 203–209 (2005).
14. Augst, S., Strickland, D., Meyerhofer, D. D., Chin, S. L. & Eberly, J. H. Tunneling ionization of noble gases in a high-intensity laser field. *Phys. Rev. Lett.* **63,** 2212–2215 (1989).
15. Corkum, P. B., Burnett, N. H. & Brunel, F. Above-threshold ionization in the long-wavelength limit. *Phys. Rev. Lett.* **62,** 1259–1262 (1989).
16. Zweiback, J., Ditmire, T. & Perry, M. D. Femtosecond time-resolved studies of the dynamics of noble-gas cluster explosions. *Phys. Rev. A* **59,** R3166–R3169 (1999).
17. Glover, T. E., Donnelly, T. D., Lipman, E. A., Sullivan, A. & Falcone, R. W. Subpicosecond Thomson scattering measurements of optically ionized helium plasmas. *Phys. Rev. Lett.* **73,** 78–81 (1994).
18. Augst, S., Meyerhofer, D. D., Strickland, D. & Chin, S. L. Laser ionization of noble gases by Coulomb-barrier suppression. *J. Opt. Soc. Am. B* **8,** 858–867 (1991).
19. Tzortzakis, S., Prade, B., Franco, M. & Mysyrowicz, A. Time evolution of the plasma channel at the trail of a self-guided IR femtosecond laser pulse in air. *Opt. Commun.* **181,** 123–127 (2000).
20. Centurion, M., Pu, Y., Psaltis, D. & Hänsch, T. W. Holographic recording of laser-induced plasma. *Opt. Lett.* **29,** 772–774 (2004).
21. Dunne, M. *et al.* Experimental observations of the expansion of an optical-field-induced ionization channel in a gas jet target. *Phys. Rev. Lett.* **72,** 1024–1027 (1994).
22. Frasinski, L. J. *et al.* Femtosecond dynamics of multielectron dissociative ionization by use of picosecond laser. *Phys. Rev. Lett.* **58,** 2424–2427 (1987).
23. MacKinnon, A. J. *et al.* Proton radiography as an electromagnetic field and density perturbation diagnostic. *Rev. Sci. Instrum.* **75,** 3531–3536 (2004).
24. Li, C. K. *et al.* Measuring E and B fields in laser-produced plasmas with monoenergetic proton radiography. *Phys. Rev. Lett.* **97,** 135003 (2006).
25. Mackinnon, A. J. *et al.* Proton radiography of a laser-driven implosion. *Phys. Rev. Lett.* **97,** 045001 (2006).
26. Corkum, P. B. Plasma perspective on strong-field multiphoton ionization. *Phys. Rev. Lett.* **71,** 1994–1997 (1993).
27. Lerner, P. B. & Cohen, J. S. Formation of hot electrons in noble gases by intense-field ionization: A quasistatic tunneling, independent-electron model. *Phys. Rev. A* **51,** 1464–1470 (1995).
28. Atzeni, S. & Meyer-Ter-Vehn, J. *The Physics of Inertial Fusion* 132–133 (Clarendon Oxford, 2004).

Acknowledgements

This work was funded in part by Deutsche Forschungsgemeinschaft (DFG) under contract SFB Transregio 6039 and by the DFG Cluster of Excellence 'Munich Centre for Advanced Photonics' (MAP; www.munich-photonics.de). M.C. is supported by a research fellowship from the Alexander von Humboldt Foundation. P.R. is supported by a scholarship from the International Max Planck Research School on Advanced Photon Science (IMPRS–APS; www.mpq.mpg.de/APS). S.A.T. thanks the Deutsche Forschungsgemeinschaft for a research fellowship (project FU 363/1).

Author information

Reprints and permission information is available online at http://npg.nature.com/reprintsandpermissions/. Correspondence and requests for materials should be addressed to M.C. and P.R.

© 2008 Nature Publishing Group